2 Supplementary Information

This section presents the Supplementary Materials and will broaden the understanding of the experimental work.

2.1 Porosity Calculation

The porosity was defined as the ratio between the volume of the pores in the electrode and the total volume of the electrode, and calculated by using Equation 1, where V is the total volume of the electrode, C is the ratio of each material in the electrode, W is the weight per area (loading) and ρ is the density of each material[1].

$$\varepsilon[\%] = \frac{V - W\left(\frac{C_{\text{NMC}}}{\rho_{\text{NMC}}} + \frac{C_{\text{Binder}}}{\rho_{\text{Binder}}} + \frac{C_{\text{Conductive additive}}}{\rho_{\text{Conductive additive}}}\right)}{V} \cdot 100 \tag{1}$$

2.2 Chemicals

Table S1 shows the list of chemicals used for cathode production.

Table S1 Detailed list of materials used and their suppliers used for the cathode production. Avg.Mw = average molecular weight.

Chemical Name and Abbreviation	Supplier	Product Number
NMC111 $LiNi_{1/3}Mn_{1/3}Co_{1/3}O_2$	Targray	SNMC03001
PVDF Poly(vinylidene fluoride)	Sigma-Aldrich Avg.Mw ~540 000 by GPC, powder	1002912638
Lignin	Sigma-Aldrich Alkali - low sulfur content (< 3.6 %) Avg.Mw ~10 000	471003
Carbon Black	Imerys Graphite and Carbon SuperP C45, TIMCAL C-NERGY™	
NMP N-Methyl-2-pyrrolidone	Sigma-Aldrich	102135677
1 M $LiPF_6$ in EC/DMC/DEC (1/1/1) Lithium Hexafluorophosphate	Sigma-Aldrich	901685

Lignin was dissolved in EC, DEC, and DMC solvents to investigate the solubility of the lignin in the electrolyte solvent used for these coin cells. Figure S1a show that the lignin was not soluble in the DMC electrolyte. Furthermore, Figure S1b shows how electrolyte wetting is problematic for cathodes containing lignin.

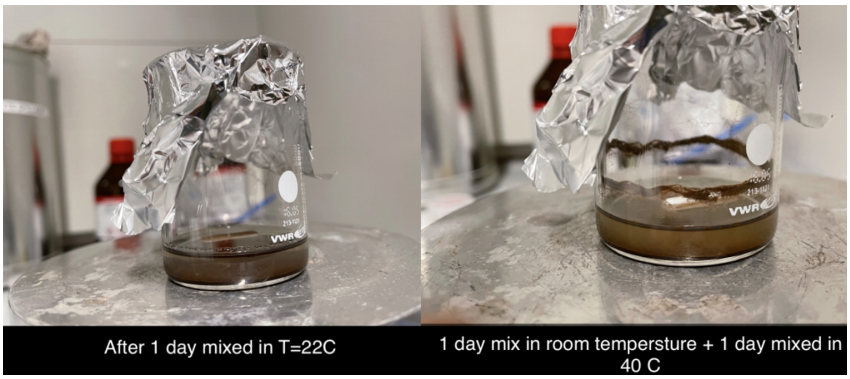

(a) Lignin powder mixed with DMC (Lignin:DMC 1:100 wt%) for a day at 22°C (left) and 40°C (right) showing the insolubility of lignin.

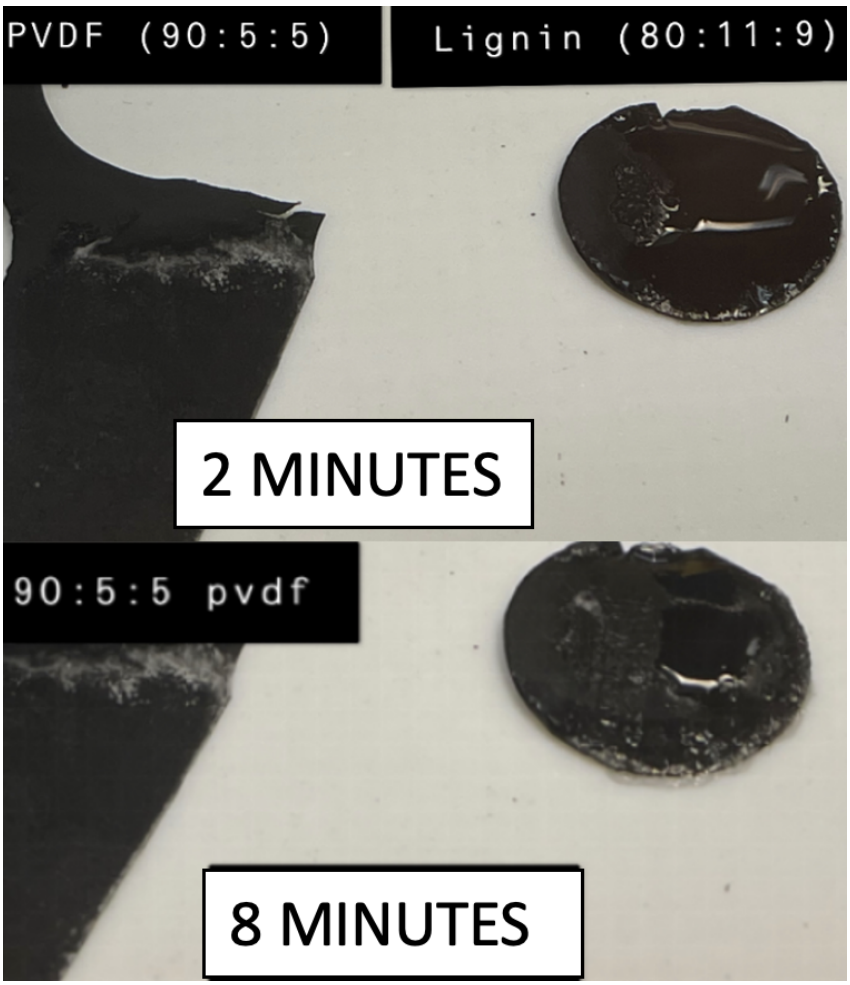

(b) Image of a drop electrolyte on two cathode surfaces after 2 and 8 minutes. Revealing wetting behavior of a PVDF-based 85:10:5 electrode-surface (left) compared to a lignin-based 80:11:9 electrode-surface (right) using 20 μL 1 M $LiPF_6$ in 1:1:1 DMC:EC:DEC electrolyte.

Fig. S1 Images showing the a) insolubility of lignin in DMC, and b) wettability of electrodes.

2.2.1 Coating Surface Analysis

This section presents the macroscopic (surface images) and microscopic (SEM analysis) for the different coatings. These data were used to investigate how the mechanical strength of the coatings, binder migration, and drying temperature affected the coatings with PVDF or lignin as a binder and NMP or water as a solvent.

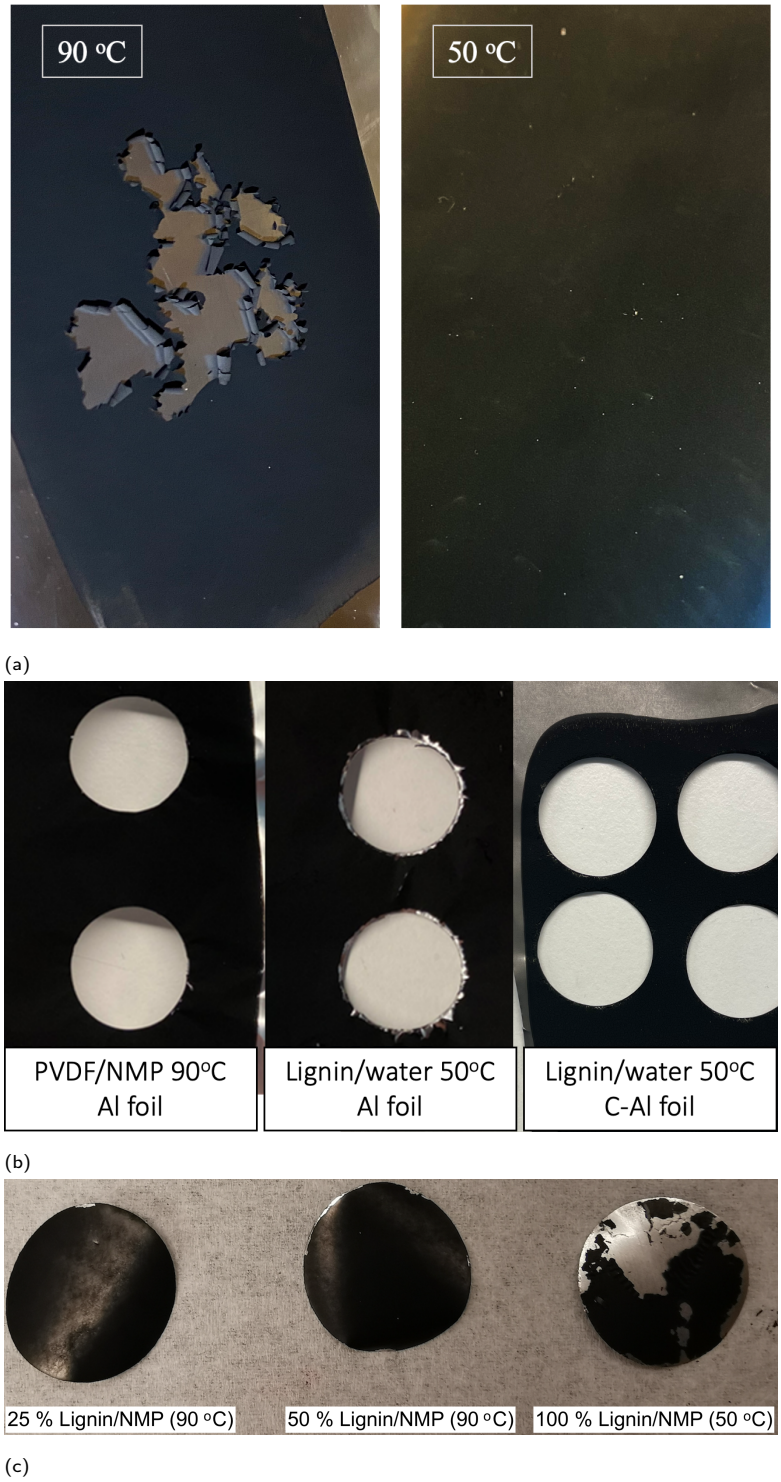

Fig. S2 (a) Lignin/NMP coated on Al after drying at 90 °C and 50 °C for 5 hours. (b) PVDF/NMP coated on Al dried at 90 °C, and lignin/water-slurry coated on Al or C-Al dried at 50 °C. (c) Calendered (PVDF/lignin)/NMP cathodes with different lignin content. Shows how calendering enhances the already poor adhesion to Al for lignin-based cells.

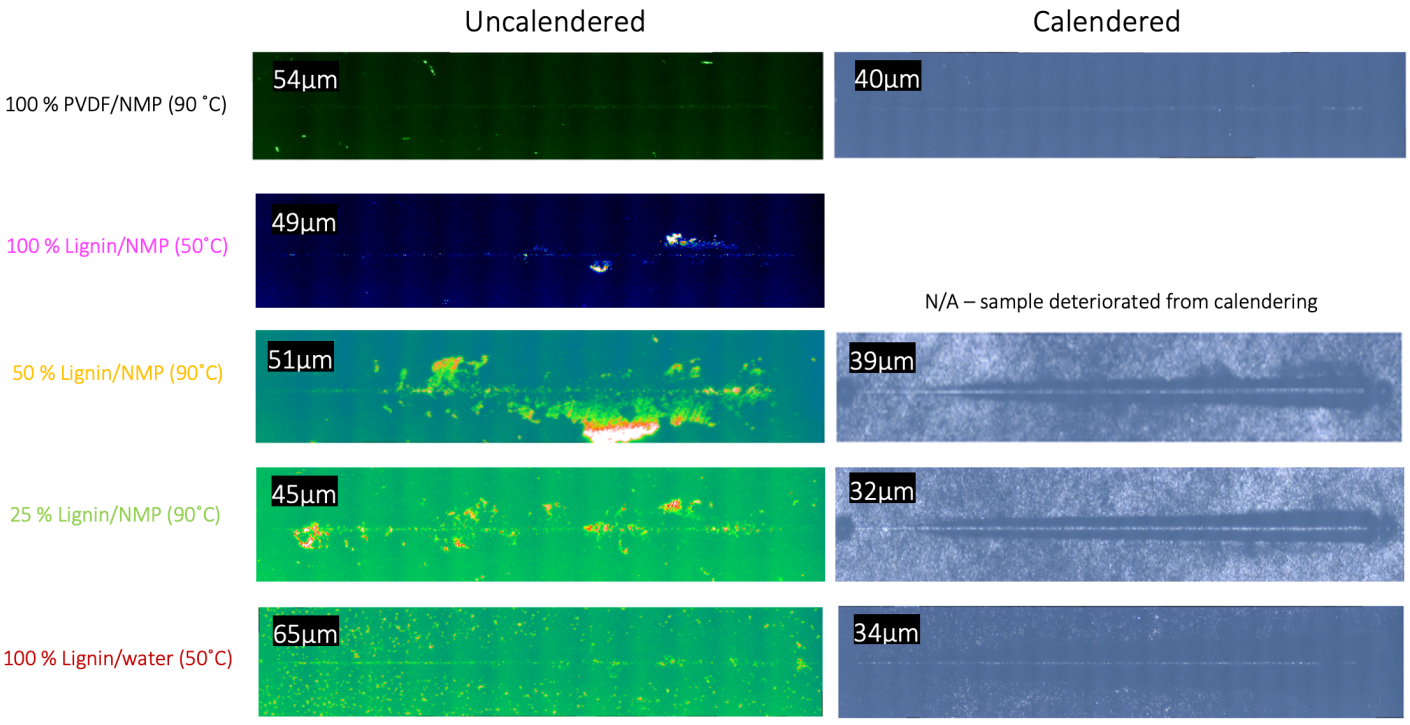

Fig. S3 Surface scratch tests of calendered and uncalendered NMC111 cathodes fabricated different binders and solvents. Showing how the different binders and drying temperatures affected the adhesion to the Al foil.

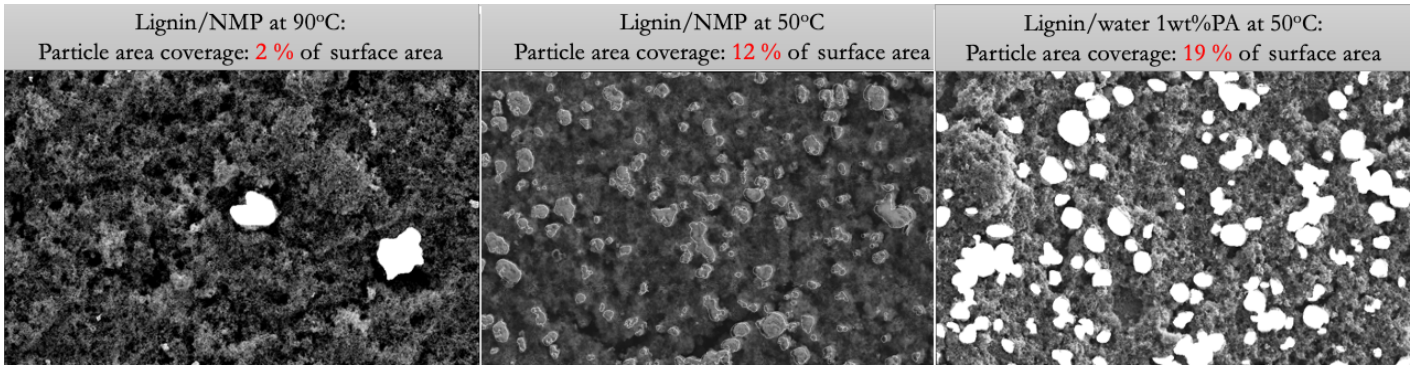

Fig. S4 The percentage of NMC particles at the surface of the electrode after NMP evaporation at 90 °C (left) and 50 °C (middle), or water evaporation at 90 °C (right). Lignin accumulation on the surface increases at high temperatures and when using water as a solvent.

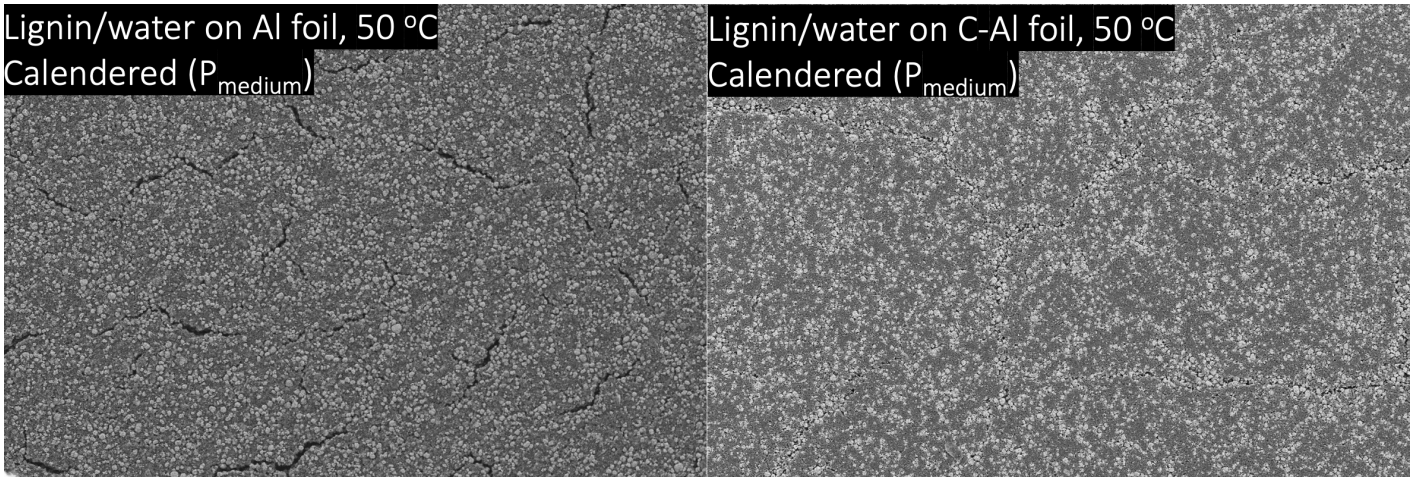

Fig. S5 SEM analysis of the surface of two lignin/water-based cathodes dried at 50 °C calendered with medium pressure (P_{medium}), using Al foil (left) or carbon coated Al (C-Al) foil (right) as a current collector. Since fewer cracks formed on the surface of lignin/water cathodes coated onto a C-Al foil versus a plain Al foil. More are detected on the Al cathode relative to that coated on C-Al even after calendering.

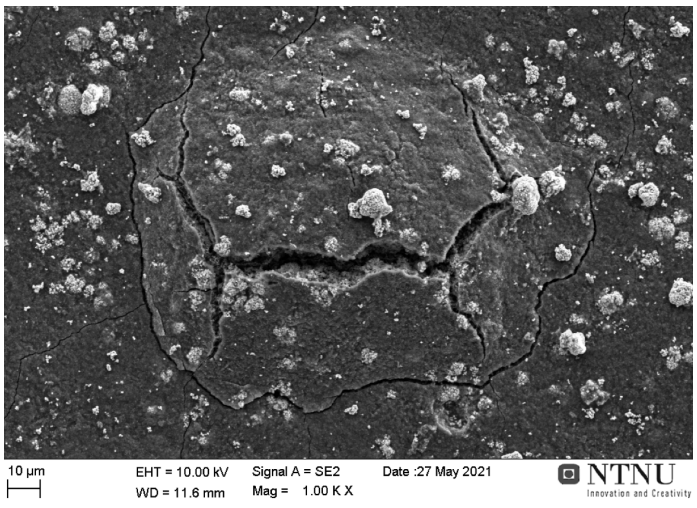

(a) Dried at 90°C

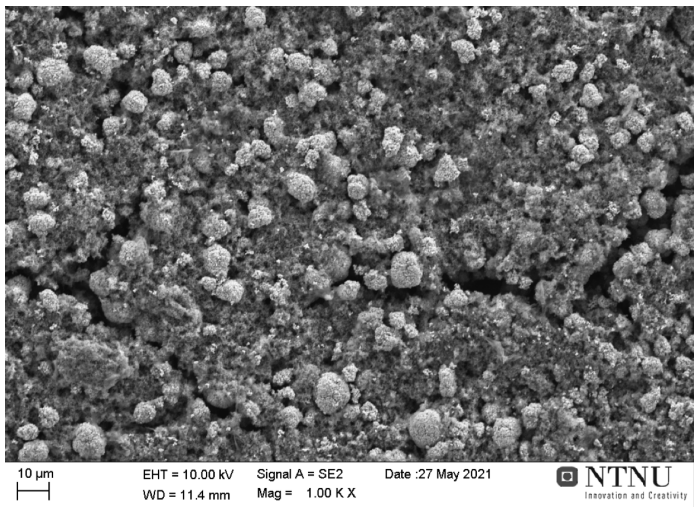

(b) Dried at 50°C

Fig. S6 Post mortem SEM of two NMC111 lignin/NMP cathode surfaces dried at different temperatures. After 3 formation cycles at C/10 and 20 cycles at C/2. Shows how the lignin accumulation on the coating surface promoted CEI layer formation.

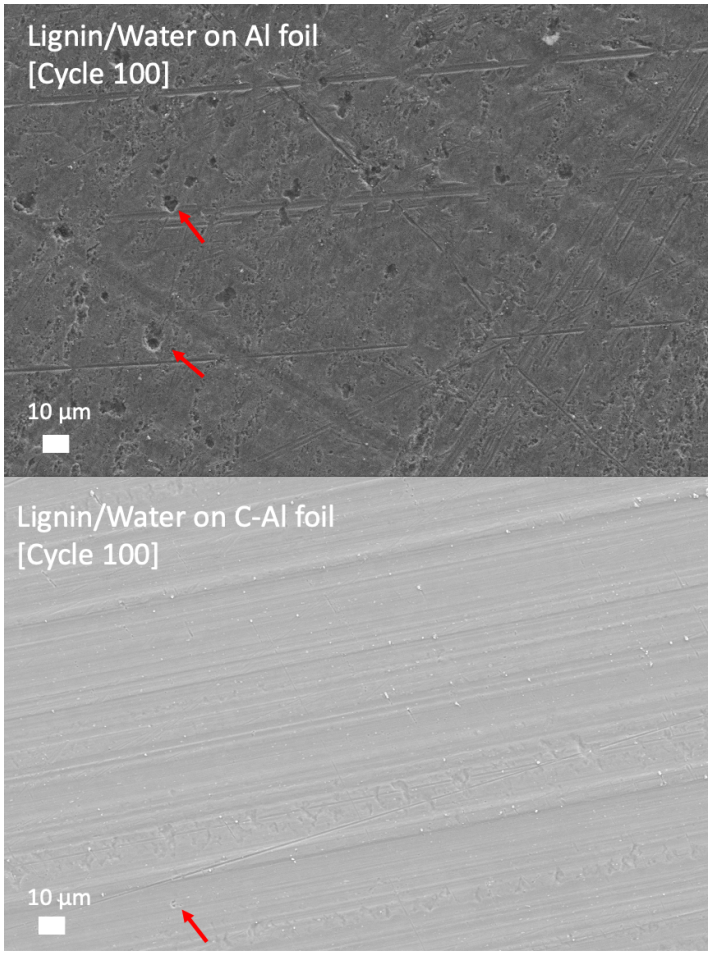

Fig. S7 SEM surface analysis of the Al foil (upper) or carbon coated Al (C-Al) current collector after 100 cycles at C/2 for lignin/water-fabricated cells. The coatings were dried at 50 °C) calendered with medium pressure (P_{medium}). They were removed using ethanol (96 %). The arrows point out examples of pit corrosion.

2.3 EDS Surface Analysis

Table S2 EDS mapping of the surface of (90:5:5) lignin/water-fabricated cathodes before cycling and after 54 cycles. Values are the normalized relative mass weight percentage [wt%] and scanned at a magnitude of 200, 500, and 1000x. An average of three scans are reported.

Sample		C [wt%]	O [wt%]	F [wt%]	Na [wt%]	Al [wt%]	P [wt%]	S [wt%]	Mn [wt%]	Co [wt%]	Ni [wt%]
Lignin/water	Uncycled	18.87±1.72	19.29±0.47	0.20±0.05	2.72±0.84	0.47±0.18	0.01±0.0	0.35 ±0.18	16.76±0.99	22.26±1.02	19.06±0.95
	54 cycles	17.20 ± 2.50	21.05 ± 3.07	7.42 ± 1.52	0.28 ± 0.02	0.04 ± 0.02	1.59 ± 0.26	0.25 ± 0.04	15.13 ± 1.84	19.86 ± 2.69	17.22 ± 2.27

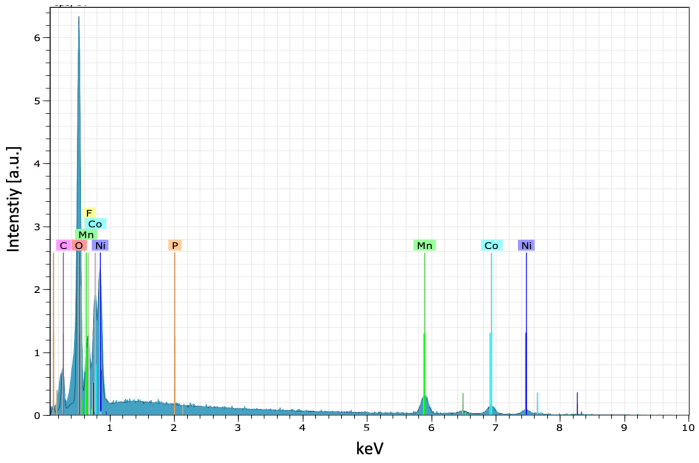

(a) PVDF, uncycled.

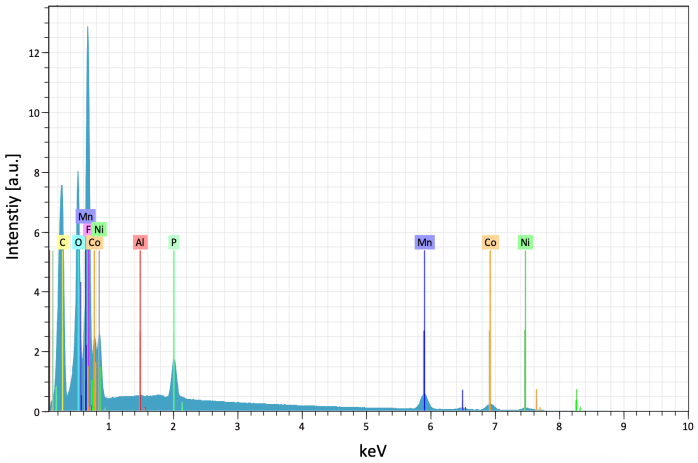

(b) PVDF, cycled.

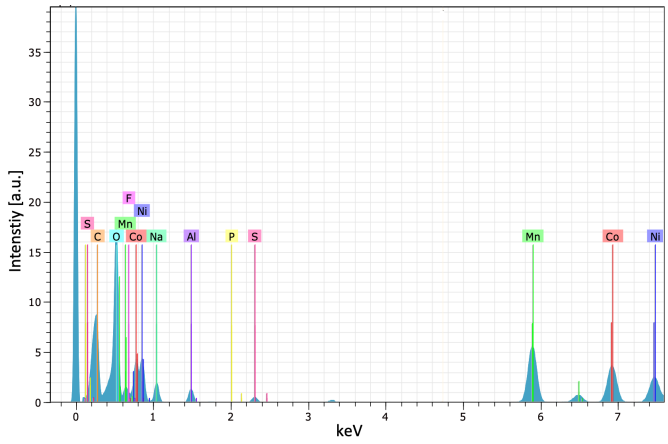

(c) Lignin/water, uncycled.

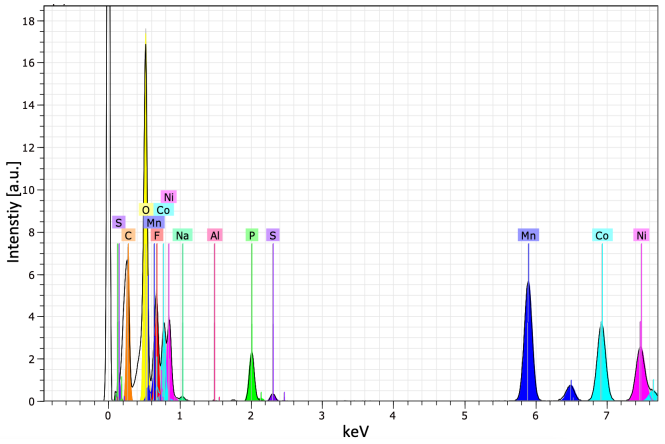

(d) Lignin/water, cycled.

Fig. S8 EDX plot of PVDF (a,b) and lignin (c,d) before and after cycling. Residuals of sodium (Na) and sulfur (S) associated with the lignin are found in lignin/water cathodes and not in PVDF/NMP cathodes. The cycled cells show residual of phosphorous (P) from the electrolyte deposition (CEI layer formation). Al was not found in the PVDF/NMP cells but in the lignin/water cells. The Al content was higher in the uncycled cells likely due to the surface cracks, which were camouflaged by the CEI layer formation after cycling. The background was removed from (c) and (d), and the normalized wt % values are summed up in Table S2.

2.3.1 Electrochemical Analysis

Additional electrochemical cycling obtained through galvanostatic measurements of coin cells are added to this section.

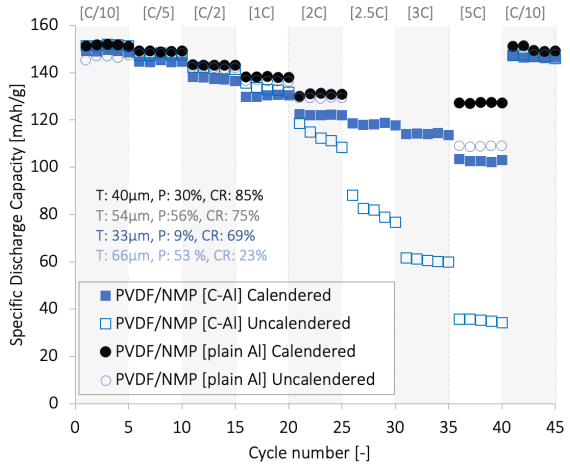

(a) Uncalendered (unfilled) and calendered (filled) PVDF/NMP-based NMC111 cathode's using Al-foil (black rings) or C-Al foil (blue squares). T_d =90 °C. T=electrode coating thickness, P=porosity, and CR=capacity retention. Mass loading: 6.6±0.6 and 6.1±0.8 mg/cm^2.

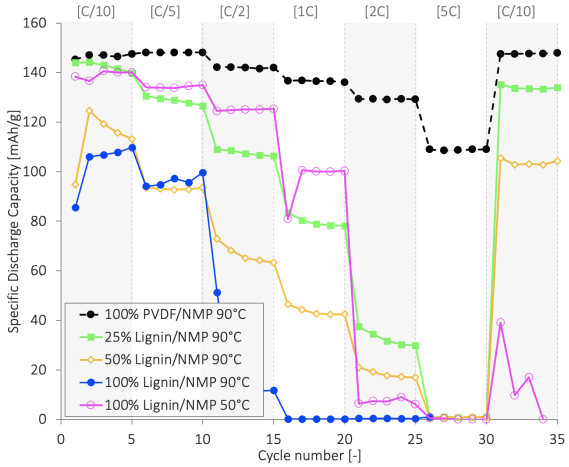

(b) Uncalendered cathodes fabricated using pure PVDF, a PVDF/lignin mix (ratio indicated by % lignin), or pure lignin. The voltage curves for the third formation cycle at C/10 are shown in Figure 8a and Figure 8b. T_d=50 °C or 90 °C. Mass loading: 4.4-4.8 mg/cm^2.

Fig. S9 Rate capability for cells produced using NMP solvent and 85:10:5 wt % NMC111:CB:binder ratio, but different binders and current collectors. a) uncalendered and calendered PVDF/NMP cathodes coated on Al-foil or C-Al-foil current collectors and b) uncalendered (lignin/PVDF)/NMP-cathodes coated on Al-foil. The coin cells were cycled between 3.0-4.3 V at C/10 (1 C = 160 mA/g) at 22°C using Li metal as anode. Cathode coatings were dried (T_d) at 50 °C or 90 °C.

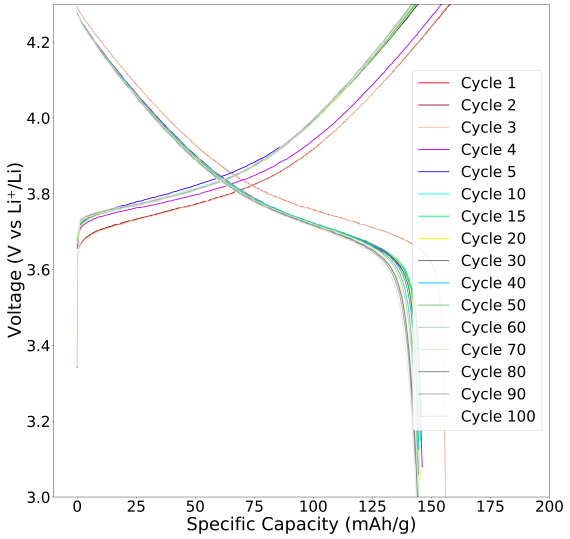

(a) PVDF/NMP based (85:10:5)

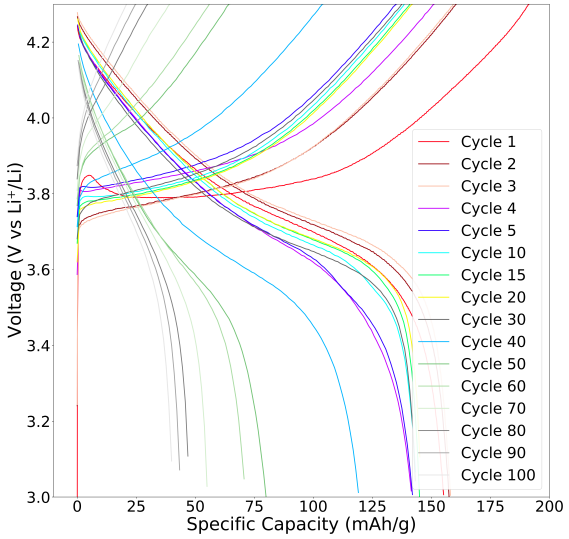

(b) Water/lignin based (80:11:9)

Fig. S10 Long-term (dis)charge curves for cathodes (NMC111:CB:binder) fabricated with different binder/solvent. a) PVDF/NMP (85:10:5), and b) lignin/water (80:11:9), both were coated onto a Al current collector. The mass loading was 3.5-4.4 mg/cm^2. The coin cells were cycled between 3.0-4.3 V at C/10 (1 C = 160 mA/g) at 22°C using Li metal as anode.

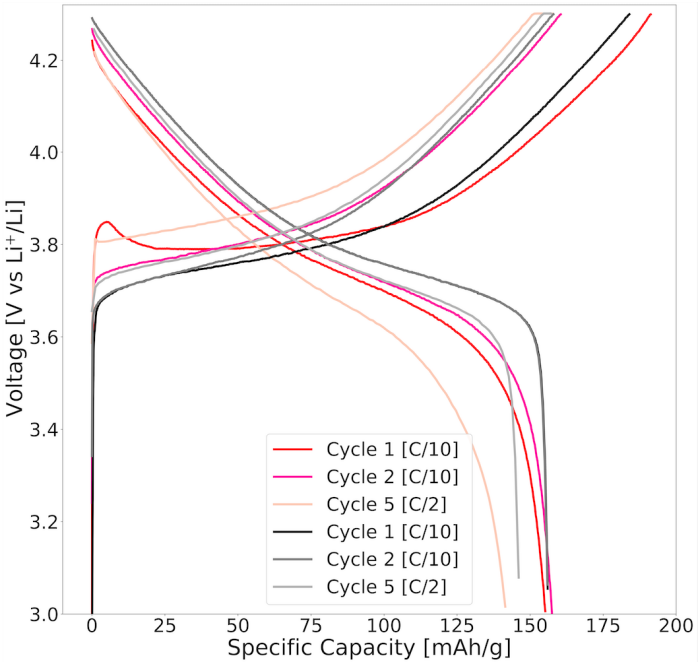

Fig. S11 The voltage profile of the first and second cycle at C/10 and the fifth cycle at C/2 for NMC111 cathodes fabricated using 80:11:9 (red)lignin/water (7.4 mg/cm^2), and 85:10:5 PVDF/NMP-fabricated cathodes (black) (6.9 mg/cm^2). The cathodes were cycled in coin cells between 3.0 - 4.3 V (vs Li$^+$/Li) at different [C-rates] at 22°C using a Li metal anode. 1C = 160 mA/g.

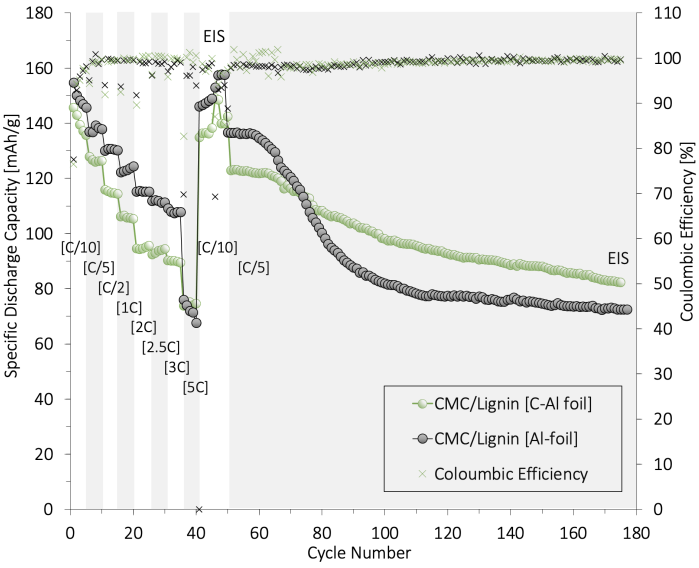

Fig. S12 The lignin/CMC aqueous produced NMC111 cathodes (80:11:9 wt % NMC111:CB:lignin) using an carbon coated Al-foil (C-Al) as a current collector (green) or a plain Al-foil (black) after 21 cycles at C/2 (squares), and 45 cycles at high rates (round), and after 177 cycles at C/2 (triangle). The first 45 cycles were discharged at different [C-rates], while the charge was kept constant (C/2). The last 130 cycles reveal the long-term cyclability at a constant C-rate (C/2). Larger cracks detected on the surface of the Al sample relative to the C-Al sample can explain why the former showed higher rate performance and lower discharge capacity relative to the C-Al with high mechanical strength.

	Lignin/Water (80:11:9) [6 days]				Lignin/Water (80:11:9) [35 days]				Lignin/Water (90:5:5) [35 days]				Lignin/Water (90:5:5) [1 day]				PVDF/NMP (85:10:5) [1 day]			
	Cycle Nr	[C-rate]	SpeDCap	CE [%]	Cycle Nr	[C-rate]	SpeDCap	CE [%]	Cycle Nr	[C-rate]	SpeDCap	[CE [%]	Cycle Nr	[C-rate]	SpeDCap	[CE [%]	Cycle Nr	[C-rate]	SpeDCap	[CE [%]
Initial Cycle	Cycle 1	C/10	143.2	75.3	Cycle 1	C/10	141.6	73.7	Cycle 1	C/10	152.0	81.6	Cycle 1	C/10	152.2	76.3	Cycle 1	C/10	152.7	81.2
	Cycle 2	C/10	145.4	96.1	Cycle 2	C/10	142.4	93.5	Cycle 2	C/10	152.1	95.2	Cycle 2	C/10	153.2	95.1	Cycle 2	C/10	153.2	97.3
	Cycle 3	C/10	147.1	96.7	Cycle 3	C/10	144.9	93.0	Cycle 3	C/10	152.9	96.1	Cycle 3	C/10	153.3	95.7	Cycle 3	C/10	153.7	98.1
	Cycle 4	C/10	148.0	97.2	Cycle 4	C/2	122.0	88.1	Cycle 4	C/10	154.0	93.7	Cycle 4	C/10	154.6	98.1				
	Cycle 5	C/10	149.3	98.6	Cycle 5	C/2	123.1	99.7	Cycle 5	C/10	153.9	98.3	Cycle 5	C/2	141.7	93.4				
	Cycle 6	C/2	132.9	86.9					Cycle 6	C/2	142.0	92.9								
Capacity peak [C/2]	Cycle 63	C/2	140.9	98.3	Cycle 33	C/2	132.1	98.5	Cycle 58	C/2	143.8	98.2	Cycle 14	C/2	136.8	99.0	Cycle 4	C/2	144.0	98.9
Avg pre-peak [C/2]	Cycle 4-63	C/2	137.7	98.7	Cycle 4-36	C/2	129.6	98.7	Cycle 6-58	C/2	142.7	98.6	Cycle 5-14	C/2	136.2	98.4				
Avg post-peak [C/2]	Cycle 64-107	C/2	118.2	97.9	Cycle 37-107	C/2	119.2	97.5	Cycle 58-107	C/2	140.8	97.8	Cycle 15-107	C/2	99.7	96.5				
Avg 100 cycles [C/2]	Cycle 6-107	C/2	137.7	98.3	Cycle 4-103	C/2	121.1	97.7	Cycle 6-107	C/2	141.8	98.2	Cycle 5-107	C/2	103.4	96.6	Cycle 4-103	C/2	142.4	99.2

Fig. S13 A summary of the coulombic efficiency (CE, %) and specific discharge capacities (SpeDCap, mAh/g) for cathodes with different solvent/binder and NMC111:CB:binder ratio.

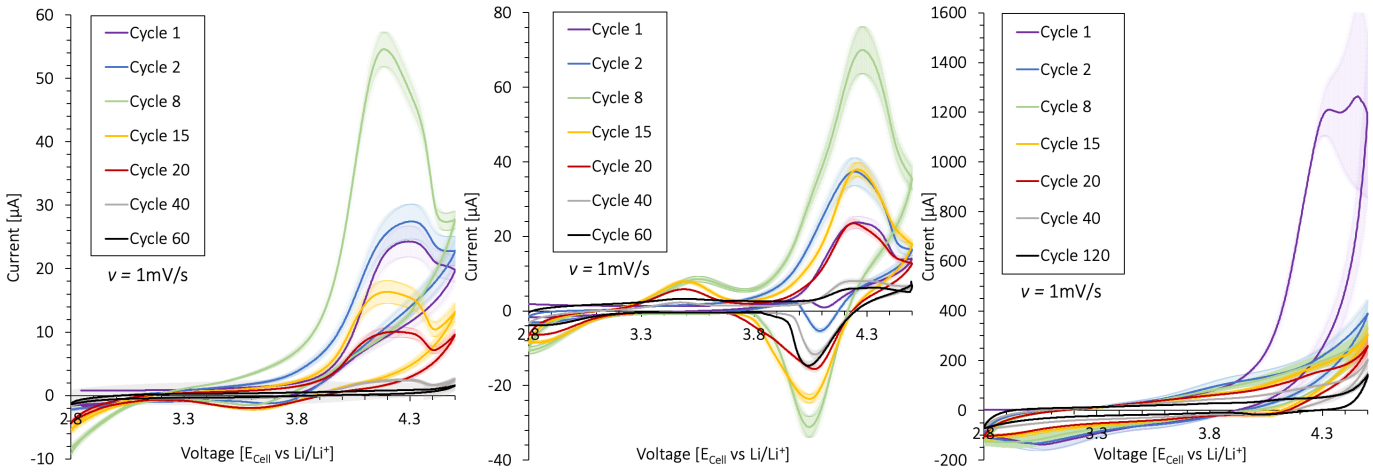

(a) Al-foil. (b) C-Al-foil. (c) Lignin/CB on C-Al, 6 days.

Fig. S14 The electrochemical activity of the a) Al-foil, b) carbon-coated Al-foil (C-Al), c) lignin/CB (50/50 wt %) coated on C-Al scanned after 6 days of electrolyte wetting. The coin cells were scanned between 2.8 - 4.5 V (vs Li/Li^+) using a Li-metal anode, $LiPF_6$ in ED/DMC/DEC electrolyte, and a scan rate of $\nu = 1$ mV/s at 22 °C.

2.3.2 XRD analysis

This section presents the XRD analysis of the lignin, PVDF, and carbon black raw materials (Figure S16) and the NMC111 powders exposed to different solvents and storage conditions (Figure S15). A Rietveld refinement was conducted on the XRD measurements for the NMC111 powders and the calculated values are presented in Table S3. The product codes of the PDF files used to identify peaks (hkl) are represented in Table S4.

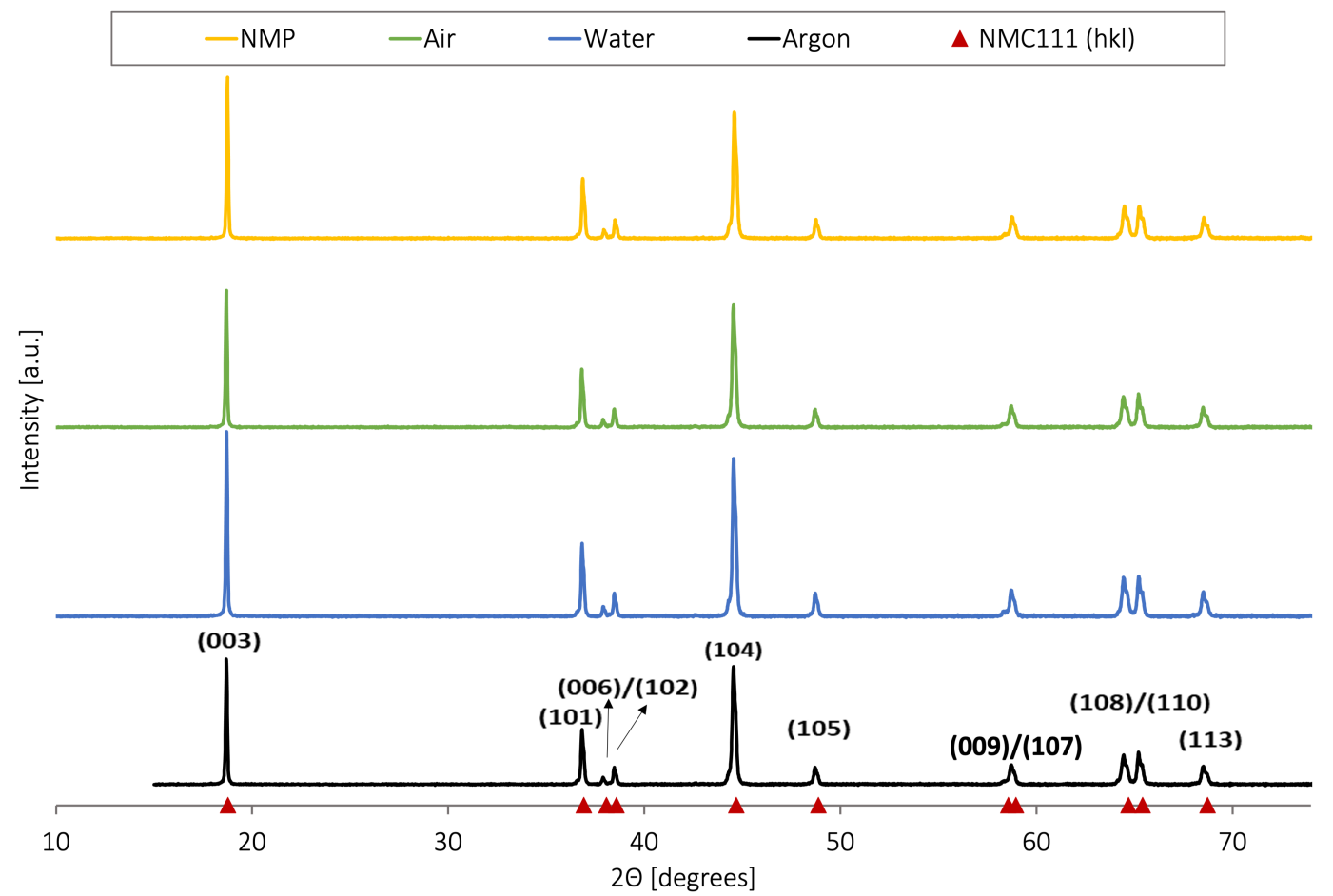

Fig. S15 XRD measurement of NMC particles exposed to different storage conditions (argon or air), solvents (water or NMP). The PDF code for the NMC111 (hkl) values are shown in Table S4. The Rietveld refinement of this XRD spectra is shown in .

Table S3 Rietvelt refined XRD measurement of pristine NMC111 powder stored in argon atmosphere (A), stored in air (B), exposed water solvent (C), and exposed to NMP solvent (D). V_a=unit cell volume, ΔV_b=volume variation relative to the pristine NMC111

Sample	Exposure	a [Å]	c [Å]	V_a [Å^3]	ΔV_b [%]	R_{wp} [%]	Ni in Li layer [%]
A	Argon	2.85892(2)	14.2360(3)	100.768(3)	0	3.01	1.99
B	Air	2.85893(2)	14.2338(3)	100.753(2)	-0.015	3.18	1.72
C	Water	2.85901(2)	14.2336(3)	100.757(3)	-0.011	3.23	1.38
D	NMP	2.85921(3)	14.2335(3)	100.771(3)	0.003	3.40	0.83

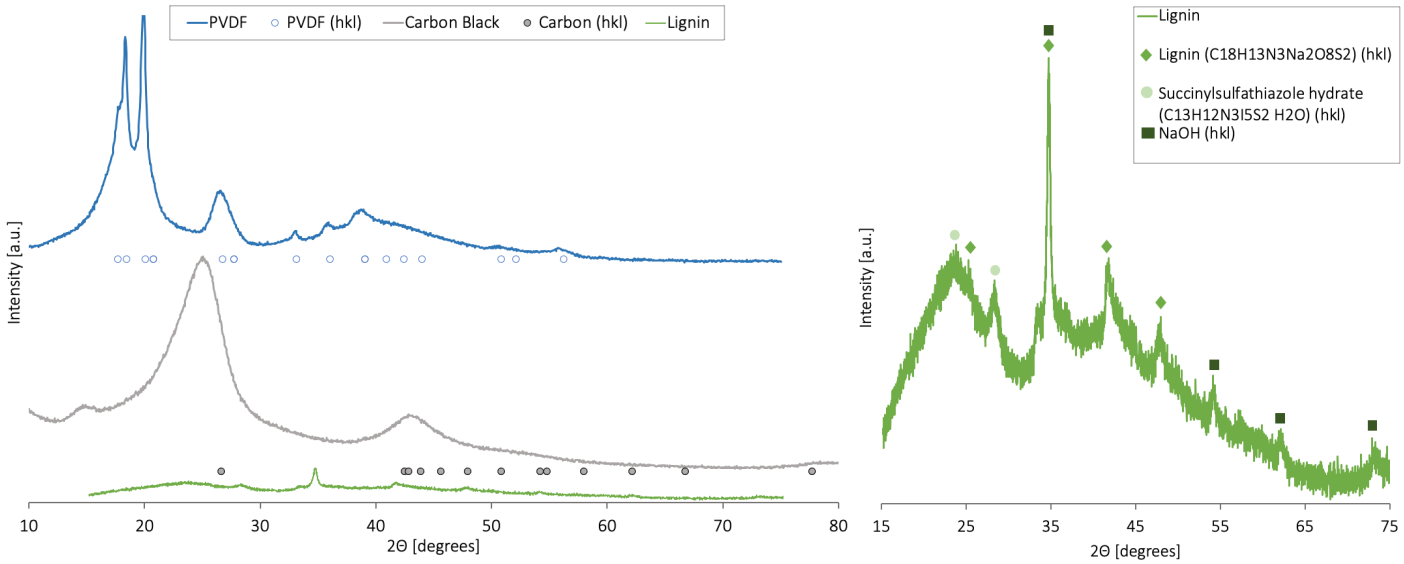

(a) PVDF, lignin, and carbon black.

(b) Lignin.

Fig. S16 XRD measurement of the lignin (green), carbon black (black), and PVDF (blue) raw materials used in the NMC111 cathode fabrication. The PDF code for the (hkl) values is shown in Table S4.

Table S4 The PDF codes used for identifying peaks in the XRD measurements.

Name	**Formula**	**PDF**
Polyvinylidene fluoride	PVDF	00-061-1406
Carbon	C	00-026-1077
NMC111	$LiNi_{1/3}Mn_{1/3}Co_{1/3}O_2$	00-062-0431
Lignin	C18H13N3Na2O8S2	00-040-1739
Succinylsulfathiazole hydrate	$C_{13}H_{12}N_3I_5S_2{\cdot}H_{20}$	00-046-1825
Sodium hydroxide	NaOH	01-081-2166

2.3.3 XPS

The XPS profiles in Figure S17 shows the surface composition of pristine NMC111 particles after being stored (for 1 year) in dry argon atmosphere (A), humid air (B), and water for 24 hours (C).

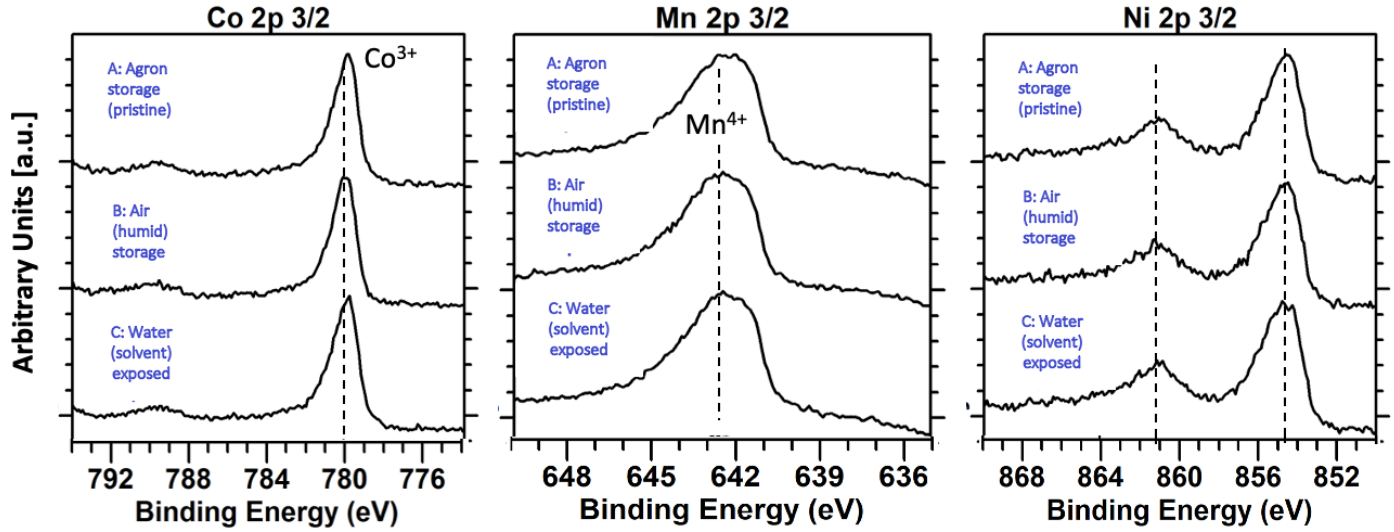

(a) Ni, Co, and Mn

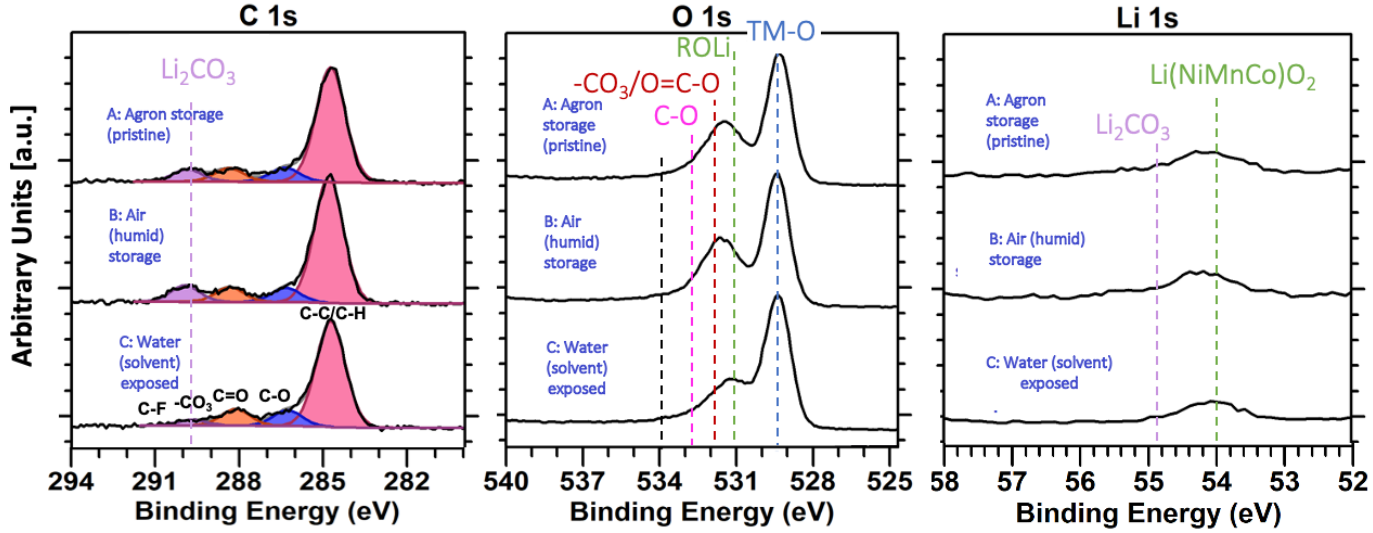

(b) C, O and Li

Fig. S17 XPS scans of pristine NMC111 powder (A), and after exposure to air (1 year) (B), or and mixed with water (24 hours).

It should be mentioned that the XRD spectra in Figure S15 showed no particular change in the bulk crystallinity of the NMC111 particles, and the changes observed in the XPS data would be associated with the NMC111 particle's surface. The peaks in the XPS spectra were assigned to different binding energies according to earlier reports[2–8].

Neither of the peaks in the transition metal (TM: Mn, Co, or Ni) spectra in Figure S17a changed when comparing the NMC111 particles stored in argon (A), humid air (B), and exposed to water (C). This indicated that the TMs were not involved in the surface layer formed upon immersion of NMC111 in water.

The main peak at 855.0 eV corresponded to Ni 2p3/2 in an oxidized form (Ni^{3+}), and its shake-up satellite was positioned at 861.5 eV. The position of the Ni 2p3/2 peak will shift to lower binding energy if the Ni^{3+}/Ni^{2+}) ratio decrease[9], meaning there was no significant reduction of the Ni^{3+} at the surface of the NMC111 particles immersed in water. The same was reported for NMC532 particles[9], whereas those with even higher Ni-contents showed the reduction of Ni^{3+} to Ni^{2+}[3]. This indicated that the proton-exchange mechanism was predominant over the redox process for NMC111 with low Ni content[9,10]. Furthermore, the intensive Co 2p3/2 peak at 780.0 eV, and its less intense shake-up satellite at 790.0

eV, were characteristic of Co^{3+} [2]. Little change was also detected in the TM-oxide bonding (TM-O) in the O 1s spectrum (Figure S17b).

Looking at the C 1s and O 1s spectra, no significant change was detected in the -CO_3 and C=O peaks for those stored for 1 year in air (B) and dry (A) atmosphere. This indicated that the formation of lithium carbonate (Li_2CO_3) surface species did not aggravate after 1 year of storage in air. This was in agreement with findings reported by Jung *et al.* [11] which also exposed NMC111 particles to air for 1 year; and the thickness of the Li_2CO_3-layer was estimated to be around 1.2-1.4 nm for pristine and air-stored NMC111 particles. This was in agreement with Wood *et al.* [4], reporting a small change in the XPS signals for the humidity exposed (B) relative to the water-exposed (C) NMC111 particles. The trace amount of LiOH and Li_2CO_3 present on the NMC111 surface initially, was suggested by Paulsen *et al.* [12] to be a result of an equilibrium coverage. This equilibrium soluble base content (SBCe) was necessary to stabilize the surface of NMC particles at the end of the particle synthesis. In fact, the removal of SBCe may deteriorate the particle surface structure and cause poor electrochemical performance, while a high content may also inflict the electrochemical performance negatively [12].

The same was true for water-exposed particles (C), although the -CO_3 peak decreased and the C=O peak was more dominant. The small differences between the NMC111 powder stored in a dry atmosphere (A) compared to those exposed to humid air (B) and water (C) supported earlier findings [4,11,13] stating that the Li_2CO_3 and lithium hydroxide (LiOH) surface contaminates formed upon humidity exposure was not thick enough to block the signals originating from TMs. Since the penetration depth of these XPS signals was at least 2-5 nm, the thickness of the Li_2CO_3 surface layer on the humidity-exposed (B) and water-exposed (C) NMC111 particles were presumably below 10 nm, which was the value estimated by Zhang *et al.* [13].

2.4 Additional Report - Phosphoric Acid Addition

Rather than protecting the Al-foil from corrosion during the aqueous production of NMC111 cathodes by using a carbon coating (C-Al), one can prevent the pH increase by adding phosphoric acid (PA) as shown in the pH measurement (Figure S19). PA was can be added as a protective coated layer around the NMC111 particle to replace the Li_2CO_3, and LiOH surface layers[14].

1 wt % PA was tested as a pH controller and an NMC111 particle coating for the lignin/water-based cathodes. An extensive elaboration on the effect of PA-additive on the performance of the lignin/water-based cathode, including the XPS measurement confirming the formation of a PA layer on the PA-coated NMC111 is presented.

The PA was coated onto the NMC111 particles according to the procedure introduced by Sahni *et al.*[15], and used as a pH controller as described by Loeffler *et al.*[16].

The XRD analysis of the pristine argon stored NMC111 particles confirmed that the PA phase detected in XPS was on the surface and that the bulk material remained intact during the coating step (Figure S21).

2.4.1 Theory

Multiple acids such as phosphoric acid (PA)[6,15,16], polyacrylic acid (PAA)[5,17], formic acid (FA)[16], and other additives[18] have successfully served as pH controllers by decreasing the slurry's pH to within the stability window of aluminum(Al)-foil. Some of these have also been used as protective NMC particle coatings to replace the LiOH, $LiHCO_3$, and Li_2CO_3 layers on the water-exposed NMC111 particles Figure S18.

PA (H_3PO_4) is amongst the most successful additives, both as a pH controller[5,9,16] and as a protective Li_3PO_4-coating for Ni-containing particles[6]. Loeffler *et al.*[16] used 1 wt % PA as a pH controller during the aqueous fabrication of NMC111, and found that the PA-controlled cathode outperformed the acid-free and those using FA acid.

Most research focuses on the influence of humid and water exposure after the cathode fabrication rather than direct water exposure during the actual processing steps. Wood *et al.*[4] investigated the influence of pH control during the aqueous processing of multiple NMC cathodes with different Ni content. They detected a subsequent increase of the pH and Li^+-leaching with high Ni content. This effect was diminished by adding a pH controller. Thus, pH-controlled NMC811 cathodes fabricated in water were cycled over 1000 times in pouch full-cells and obtained capacity retention ($\sim$70 %) similar to NMP-processed cells ($\sim$76 %).

Others has surface coated NMC111[19], NMC622[19], and NMC532[15] particles with a protective Li_3PO_4 layer. Jo *et al.*[19] successfully formed Li_3PO_4 coatings on NMC622 particles by mixing them with anhydrous PA dissolved in ethanol, followed by a heat treatment during which H_3PO_4 reacted with residual LiOH, Li_2O, and Li_2CO_3 on the surface of NMC622, according to equations shown in Figure S18[19]. The PA-coated NMC622 particles improved the electrochemical performance of the cathode. Sahni *et al.*[15] used the same method to coat NMC111 particles with PA, and reported that the specific discharge capacities increased from 130 mAh/g for the cathodes using pristine NMC111 to 177 mAh/g for the PA-coated NMC111 at C/10. Additionally, the capacity retention for the pristine NMC111 cathodes after 100 cycles at 1C was $\sim$45% (58 mAh/g), whereas the corresponding capacity retention for the PA-treated NMC111 was $\sim$67% (120 mAh/g).

The enhancement in initial discharge capacity, capacity retention, and rate capability for PA-coated NMC111 cathodes was attributed to several different mechanisms[19]. Firstly, the insulating residual Li-containing compounds (Li_2CO_3 and LiOH) on the NMC surface were replaced with an ionic conductive ($6{\cdot}10^{-8}$ S/cm) PA-layer[19]. The rate capacity; therefore, mainly increased through the enhancement in Li^+-transport that allowed for proper Li^+-(de)intercalation at the electrode/electrolyte interface during charge and discharge. Secondly, the PA coating minimized the formation of a layered-to-spinel phase transition in the NMC111 particle surface, which avoided the loss of active material for charge storage and increased the initial capacity. However, this effect was small since the thicknesses of the surface reduced layer, and the disordered spinel structure on the surface region was only a few nanometers[15,20]. Another critical effect explaining the enhanced long-term performance of PA-coated NMC particles was the prevention of Al corrosion. Furthermore, PA's ability to absorb water in the electrolyte prevented the NMC from undergoing deleterious side reactions with HF from the $LiPF_6$ electrolyte[19].

Despite the benefits of applying acids, challenges remain. These include promoted Li^+-leaching, dissolution of the transition metals (TMs: Ni, Co, and Mn)[9,15,21,22], and a decreased adhesion to the Al current collector as the acid rapidly occupies Al's oxygen sites and blocks the binder interaction[17]. In both water and acidified water, the dissolution trend of NMC111[16] and NMC532[9] are Li $\gg$ Ni $>$ Co $>$ Mn. The dissolution of TMs in acidic solutions may increase by 100, but it

is still an order of magnitude below the Li-dissolution (2.5 %).

2.4.2 Side Reactions with Kraft Lignin

Side reactions can occur between the alkali residuals from the kraft lignin (such as NaOH and Na_2S) and the phosphoric acid (PA) during the aqueous slurry production. The main reaction paths are illustrated in Figure S18.

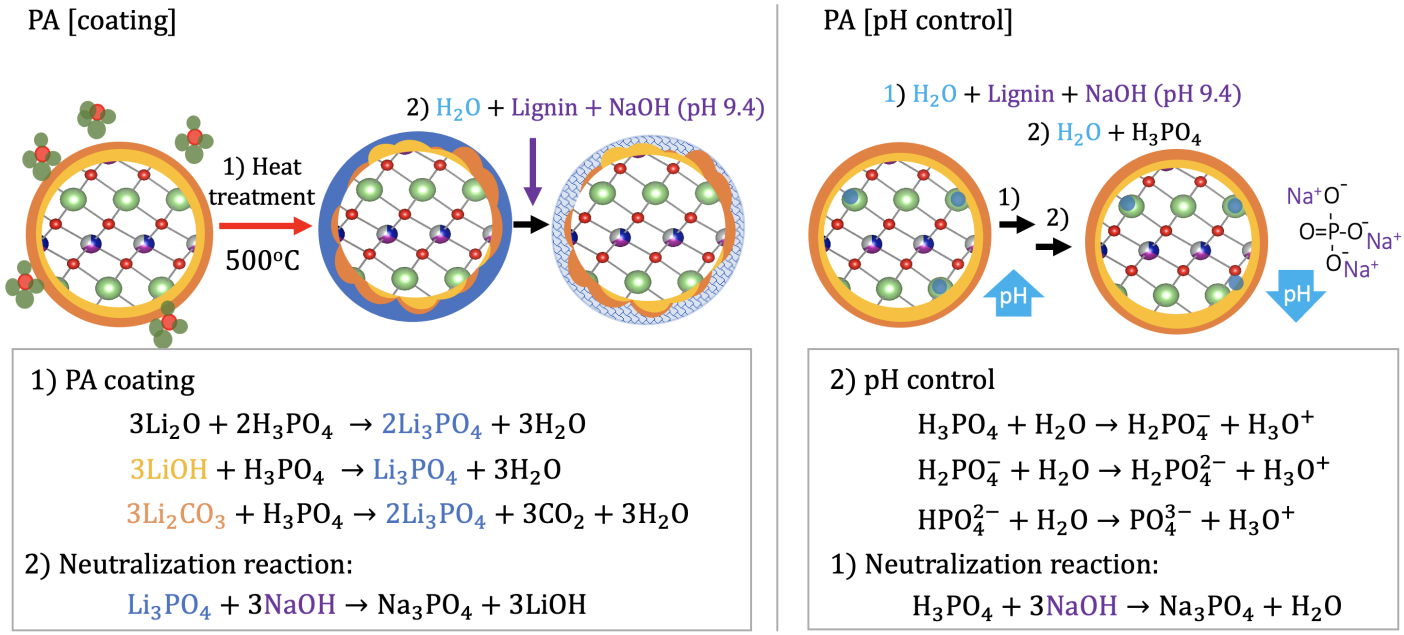

Fig. S18 By adding H_3PO_4 (PA), followed by a heat-treatment, H_3PO_4 reacts with LiOH, Li_2O and Li_2CO_3 to form a protective Li_3PO_4–coating on the NMC111 particle surface. Upon exposure to the dissolved kraft lignin containing NaOH, coating degradation and formation of LiOH may occur. When mixing the PA into a lignin/water-based slurry to lower the pH and protect the Al coating from corrosion, the lignin may react to NaOH and form Na_3PO_4.

When using PA as pH controller, the PA was in the form of H_3PO_4 before being exposed to the lignin/water-slurry. When PA was mixed with the pre-dissolved lignin solution (1:10 wt % lignin:water), reactions (2) and (3) may occur.

$$H_3PO_4(aq) + 3\,NaOH(aq) \Leftrightarrow Na_3PO_4(aq) + 3H_2O(aq) \quad (2)$$

$$Na_2S(aq) + H_3PO_4(aq) \Leftrightarrow Na_3PO_4(aq) + 3H_2S(aq)(aq) \quad (3)$$

Since the pH was 9.4 and the NaOH was present in a low concentration, the complete formation of Na_3PO_4 was unlikely. EDS in Table S2 and the pH rise indicated that the concentration of NaOH was higher than the Na_2S; thus, the (1) occurred to a larger extent.

When PA was pre-coated onto the NMC111 before the exposure to the lignin slurry, PA was in the form of a solid Li_3PO_4-layer. Upon NaOH exposure, this layer could dissolve into Na_3PO_4 and LiOH.

$$Li_3PO_4(s) + 3\,NaOH(aq) \Leftrightarrow Na_3PO_4(aq) + 3LiOH(aq) \quad (4)$$

Monobasic sodium phosphate NaH_2PO_4 has been examined as an electrolyte additive to mitigate Mn dissolution in $LiMn_4O_2$ cathodes for lithium-ion batteries[23]. Furthermore, $NaPO_4$ has been used as a particle nano-coating for sodium batteries due to its high ionic conductivity for Na^+ (r=0.102 nm). Therefore, this compound may also provide sufficient high conductivity for Li^+ (r=0.076 nm) with a lower atomic radius (r).

2.4.3 Results

pH measurement

Considering that NMC111 particles may experience Li^+-leaching and corrosion of the Al-foil, pH measurements were conducted in water+NMC111 and water+lignin+NMC (slurry) mixtures with 1 wt% phosphoric acid (PA). These are shown in Figure S19. The Figure S19b also shows the order of which the components were added for the lignin/water-slurry and the species present in the mixture.

All mixtures stabilized at a pH $>$ 10 within the first minute except those exposed to PA, which was kept within the stability window of the Al foil (a gray area in Figure S19) for up to 6 hours. After that, the pH approached 9 after 24 hours, and 6 hours were considered the time limitation for the mixing, coating, and drying step when using PA as a pH controller in these cathodes. The SEM surface analysis of the Al-foil conducted with and without PA-addition in Figure S25 revealed that the corrosion of the Al-foil decreased when using PA as a pH controller during the aqueous production.

Additionally, the pH and temperature were measured during the PA-coating procedure (Figure S23). An explanation on the coating procedure are found in Figure S23.

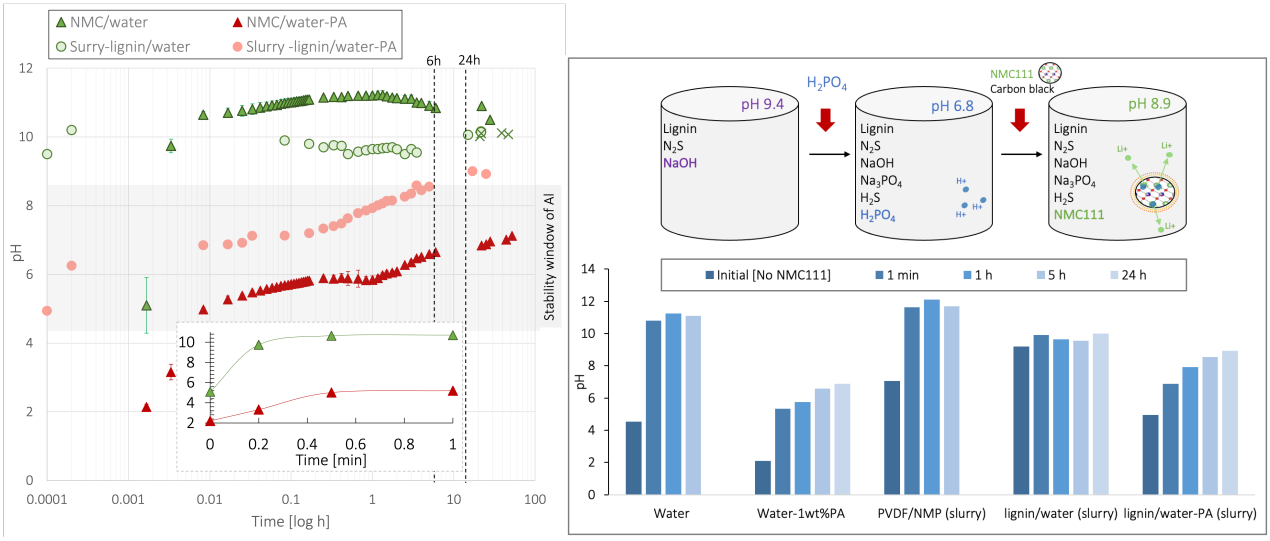

(a) (b)

Fig. S19 The pH measurement during the mixture of water or water+ 1wt%PA mixed with a low concentration of NMC111 powder (11.45 wt%) or as a slurry (80:11:9):1.7 wt % (NMC111:CB:lignin):water at 22 °C. The point measurements display the average of two measurements, and the points denoted "x" are measurements taken after adding extra water to the lignin/water slurry. The illustration shows the order in which components were added for the lignin/water-PA (slurry) sample.

XPS of PA-coating

Table S5 NMC111 particles exposed to different conditions, with the expected and detected surface species from Supplementary Figure S20b and Figure S20a

Sample	Conditions	Expected	Detected
A	Pristine (argon storage)	No phases	
B	Pristine (air storage)	Low amounts C, $LiCoO_3$, and LiOH	
C	Water solvent exposed	High amounts C, $LiCoO_3$, and LiOH	
D	NMP solvent exposed	No phases	
E1	PA-exposed (overnight at 80 °C)	H_3PO_4 or Li_3PO_4	
E2	PA-coated (5h at 500 °C)	Li_3PO_4 and low C, $LiCoO_3$, and LiOH	

The XPS profiles in Figure S20 confirmed the formation of the PA surface coating[9]. The PA-exposed (E1) and the final heat-treated PA-coated (E2) NMC111 powders showed a decrease in the –CO_3 peak resembling Li_2CO_3 and C-C/C-H, meanwhile traces of phosphorous in P 2p in Figure S20b was found on the surface. According to the O 1p spectrum (Figure S20b), the NMC111 particles exposed to PA with a heat treatment at 500 °C (E2) matched with the binding energy of Li_3PO_4 (534 eV). The aforementioned indicated that the Li_2CO_3 surface layer was partially replaced with Li_3PO_4 according to the right-sided equations in Figure S18.

The penetration depth of the XPS signals used here was at least 2-5 nm, and might be even deeper for relative light

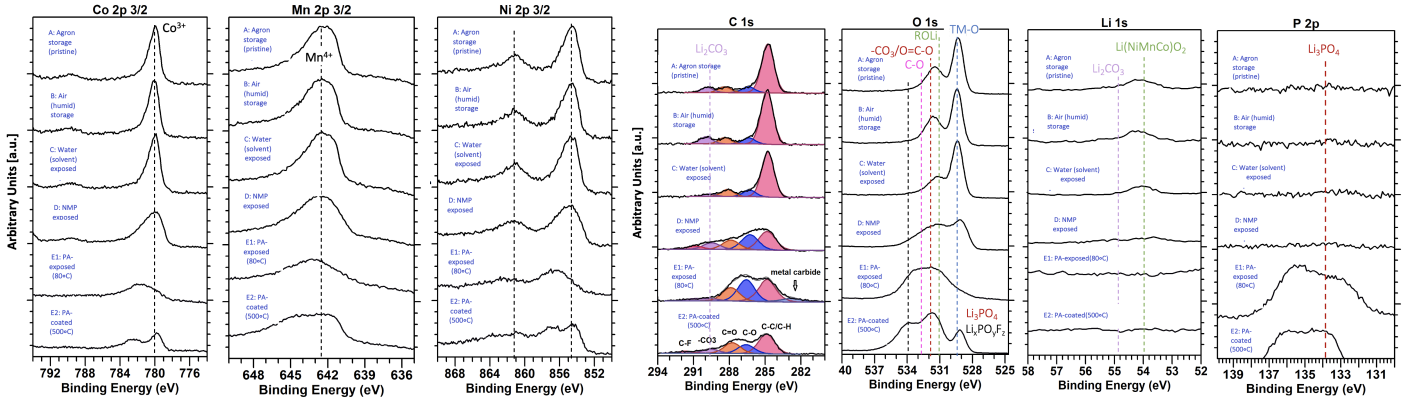

(a) (b)

Fig. S20 XPS scans of pristine NMC111 powder (A), and after exposure to air (6 months) (B), water (overnight) (C), NMP (overnight) (D), exposed to PA during the first heat-treatment (80°C) during synthesis of the PA-coating (E1), and after the last heat treatment (500 °C) and the formation of the PA-coating (E2)

materials such as NMC111. The thickness of the PA coating was calculated from the surface area of NMC111 (0.45 m^2/g), the mass of PA (1 wt % of the NMC111), and the density of PA (1.88 g/cm^3) to be 1.9 nm. Thus, the detected XPS signals were likely generated from both the PA coating and the bulk of an NMC111 particle.

Furthermore, signals from TMs (Ni, Co, and Mn) in Figure S20a were weaker for the PA-coated NMC111 particle compared with the water-exposed NMC111 particles. The weak TM signals indicated that either 1) the PA surface coating was thicker than the Li_2CO_3 surface contamination layer formed during water exposure leading to weaker TM signals from the NMC111 bulk, or 2) the dissolution of TMs had occurred on the surface in the presence of PA. Previous studies have reported that acidic additives such as PA and formic acid (FA) promote Li^+-leaching and TM dissolution[15,21]. Both a thick surface resistance layer and TM dissolution can explain the low initial discharge capacity (IDC = ≈100 mAh/g) for cathodes formulated with PA-coated NMC111 particles in Figure S22.

The Li_2CO_3-peak intensities in the C 1s spectrum for the water-exposed (C) and the pristine (A) NMC111 particles indicated a thin coverage of the contaminating surface layer for the former. The reaction with water may need to be more prevalent and form a thicker Li_2CO_3 and LiOH surface layers than the layer formed on these NMC111 particles for the PA-coating to sufficiently improve the capacity.

XRD of PA-coating

Table S6 Rietvelt refined XRD measurement of pristine NMC111 powder stored in argon atmosphere (A), stored in air (B), exposed water solvent (C), and exposed to PA during PA-coating (80°C) and for PA-coated NMC111 (500°C). V_a=unit cell volume, ΔV_b=volume variation relative to the pristine NMC111

Sample	Exposure	a [Å]	c [Å]	V_a [Å^3]	ΔV_b [%]	R_{wp} [%]	Ni in Li layer [%]
A	Argon	2.85892(2)	14.2360(3)	100.768(3)	0	3.01	1.99
B	Air	2.85893(2)	14.2338(3)	100.753(2)	-0.015	3.18	1.72
C	Water	2.85901(2)	14.2336(3)	100.757(3)	-0.011	3.23	1.38
E1	PA-exposed (80°C)	2.85913(2)	14.2330(3)	100.762(2)	-0.006	3.06	1.80
E2	PA-coated (500°C)	2.8602158(2)	14.2378128(3)	100.872(2)	0.103	3.14	1.83

Electrochemical performance The electrochemical performance was lower for the NMC111 cathodes produced with PA than the NMC111 cathodes produced without additives. Several have reported a minimal surface layer formation of NMC111 during water exposure, which increases in thickness when moving towards NMC cathodes of higher Ni-content[4,11]. This may explain why a PA-coating improved the performance for Ni-rich cathodes; NMC622[19], NMC532[15], NMC811[4], NCA532[6]. Furthermore, it justified the high cyclability (Figure S22b) obtained when using the PA as a pH controller in the slurry production[16], rather than as a coating

The increase of specific capacity observed in Figure 12a over the first ∼25 cycles for water-exposed NMC811 cathodes has earlier been reported to be caused by the partial decomposition of carbonate species within the first cycles[11,24].

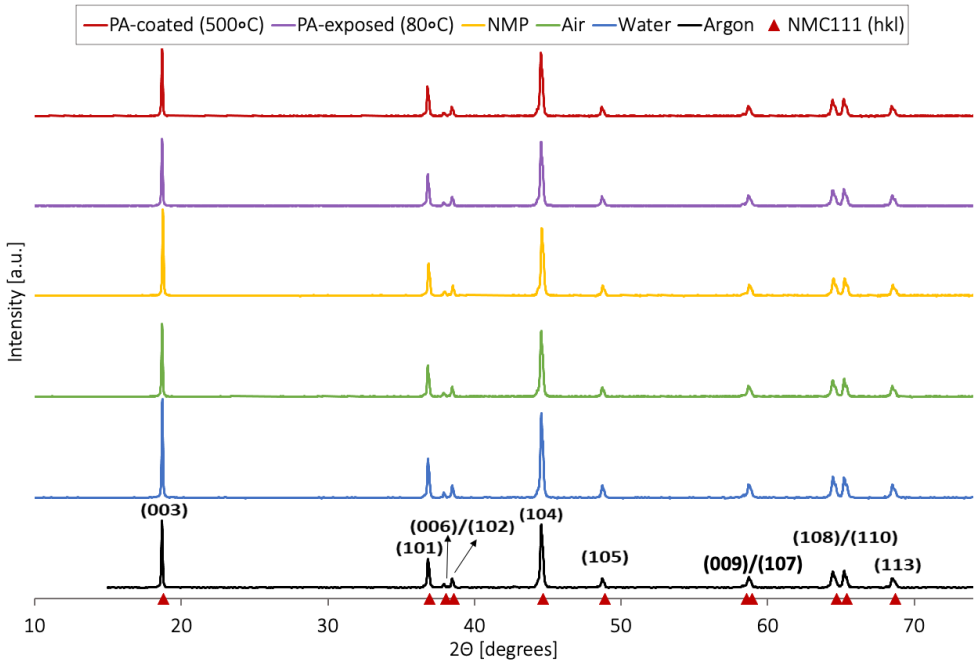

Fig. S21 XRD measurement of NMC particles exposed to different storage conditions (argon or air), solvents (water or NMP), or acidic solutions (PA-exposed after the 80 °C heat treatment, and PA-coated after 500 °C heat treatment). The NMC111 (hkl) PDF: 00-062-0431. The Rietveld refinement of this XRD spectra is shown in Table S6.

However, the PA-exposed NMC111 particles without such surface carbonates showed a similar falling trend (Figure S24), which confirmed the decreasing capacity in the first cycles being a result of the poor wetting of lignin.

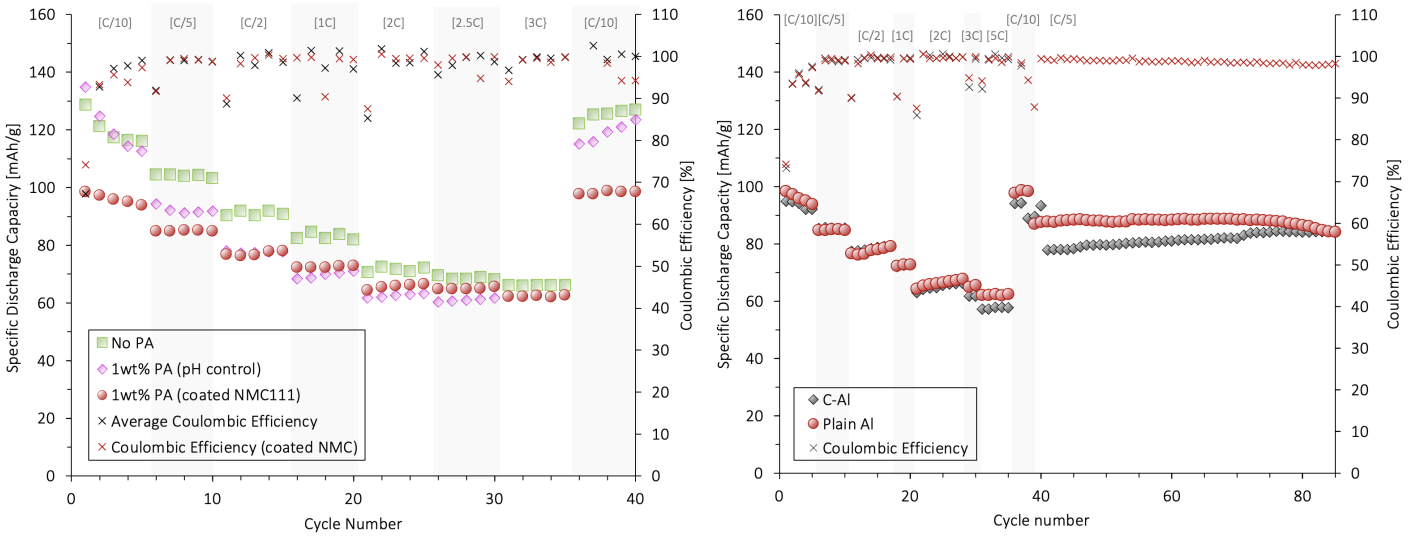

(a) (b)

Fig. S22 Rate performance (a) and long-term cyclability (b) for lignin/water-cathodes (80:11:9 wt % NMC111:CB:lignin) coated onto an Al foil and calendered with P_{medium}. Without PA (green) additive, with PA as pH controller (pink), and with PA-coating. A C-Al-foil current collector was also tested (black). The cathodes were cycled at different [C-rates] where 1 C = 160 mA/g in coin cells between 3.0 - 4.3 V (vs Li^+/Li) against a Li metal anode at 22 °C. These cathodes were wetted for 6 days before cycling, and had a mass loading: 10-11 mg/cm^2, thickness: 50-57 μm, and porosity: 7-9 %.

Figure S22 shows that the cathodes coated on a pure Al, formulated using PA-coated NMC111 had a lower initial capacity (99 mAh/g) compared to those with PA as pH controller (135 mAh/g) and those without PA ($\sim$ 140 mAh/g).

The main contribution to the decrease in specific capacity in the presence of PA is more likely the reaction with NaOH from the alkali lignin during the slurry mixing (causing the high initial pH for lignin/water slurries in Figure S19). When adding PA as a pH controller, H_3PO_4 may react with NaOH trough a neutralization reaction to form LiOH and Na_3PO_4 according to Equation 2. When using a PA-coated NMC111, the NaOH may have dissolved the Li_3PO_4-coating as proposed in Equation 4. Additional post-mortem studies should be conducted in future studies to establish an understanding of the potential degradation of this layer.

A second reason may be that the PA coating created a thicker surface layer than the Li_2CO_3 contamination formed on the NMC111 particles during water exposure, as indicated by the XPS measurements since TM signals were blocked for PA-coated particles, but not for the water-exposed with Li_2CO_3. A thicker layer increased the resistance for Li^+-intercalation.

Lastly, the acid may have promoted partial dissolution of TMs from the NMC111 particles[22] or decreased the adhesion to the Al foil[17]. Low adhesion to the plain Al current collector in the presence of PA may explain why the capacity of PA-containing cathodes coated onto an Al foil started declining after 100 cycles in Figure S22b, while the capacity for cathodes coated onto a C-Al increased.

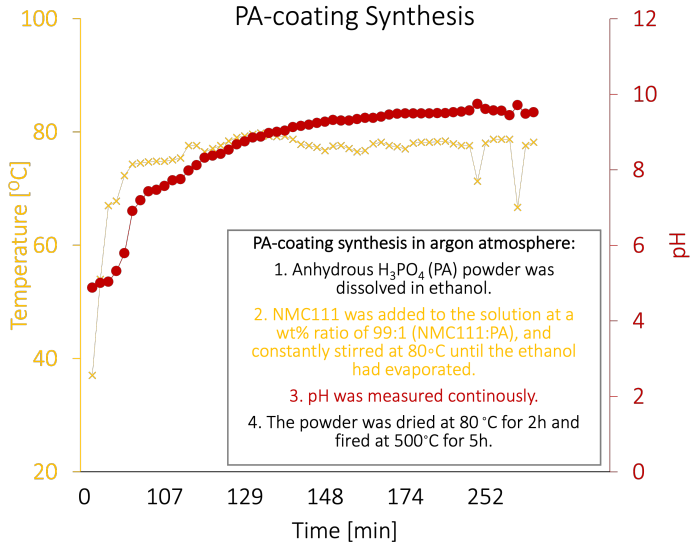

Fig. S23 Synthesis of the PA coating, and the pH and temperature measurement.

2.4.4 Conclusion

H_2PO_4 was used as a pH controller and prevented the corrosion of Al for the lignin/water-based slurries. The NMC111 particles were successfully surface-coated with Li_3PO_4 to replace the LiOH and Li_2CO_3 surface layers. The bulk crystal structure remained unaffected. The coating lowered the initial specific discharge capacity from ~140 mAh/g to 99 mAh/g. The acid may promote TM leaching, poor adhesion to the Al, or undergo side reactions with the NaOH species from the kraft lignin which may have dissolved the Li_3PO_4-coating. Furthermore, this Li_3PO_4-layer may in fact be thicker than the thin LiOH and Li_2CO_3-surface layers formed on water-exposed NMC111 particles with low Ni content, which may increase the Li^+-(de)intercalation resistance. Further investigation on this matter was out of the scope of this paper. The carbon-coated Al current collector (C-Al) was preferred over PA-control and PA-coating as a method to prevent corrosion of the Al when fabricating a lignin/water-based NMC111 cathode.

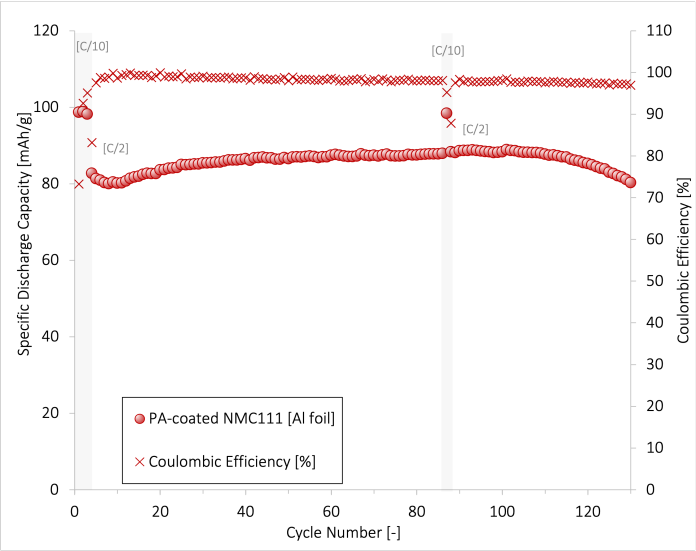

Fig. S24 Galvanostatic cycling performance over 100 cycles (at C/2) for lignin/water-cathodes fabricated with PA-coated NMC111 particles. The drying temperature was 50 °C. The cathode was wetted for 6 days before cycling, and had a mass loading: 10-10± mg/cm^2, 50-57 μm, porosity: 7-9 %.

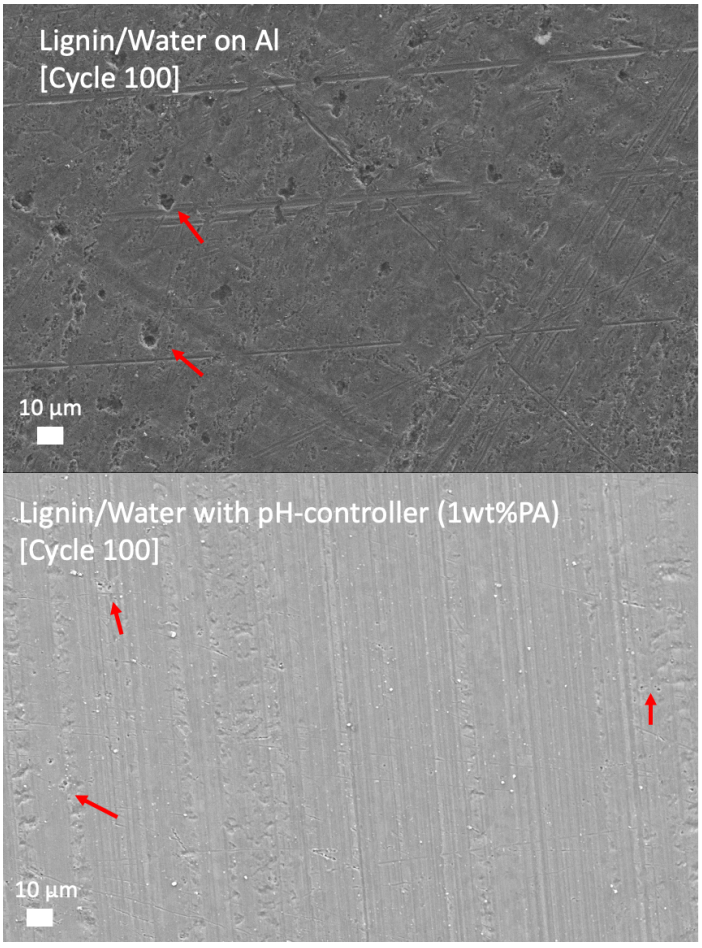

Fig. S25 SEM surface analysis of the Al current collector after 100 cycles for lignin/water fabricated cells and cells using PA-controller. The arrows point out examples of pit corrosion.

Notes and references

1 M. N. Al-Shroofy, *PhD thesis*, University of Kentucky, 2017.

2 N. V. Kosova, E. T. Devyatkina and V. V. Kaichev, *Journal of Power Sources*, 2007, **174**, 965–969.

3 K. Shizuka, C. Kiyohara, K. Shima and Y. Takeda, *Journal of Power Sources*, 2007, **166**, 233–238.

4 M. Wood, J. Li, R. E. Ruther, Z. Du, E. C. Self, H. M. Meyer, C. Daniel, I. Belharouak and D. L. Wood, *Energy Storage Materials*, 2020, **24**, 188–197.

5 W. B. Hawley, H. M. Meyer and J. Li, *Electrochimica Acta*, 2021, **380**, 138203.

6 A. Kazzazi, D. Bresser, A. Birrozzi, J. von Zamory, M. Hekmatfar and S. Passerini, *ACS Applied Materials & Interfaces*, 2018, **10**, 17214–17222.

7 N. D. Phillip, C. Daniel and G. M. Veith, *Journal of The Electrochemical Society*, 2020, **167**, 040521.

8 L. Liang, X. Sun, C. Wu, L. Hou, J. Sun, X. Zhang and C. Yuan, *ACS Applied Materials and Interfaces*, 2018, **10**, 5498–5510.

9 M. Bichon, D. Sotta, N. Dupré, E. De Vito, A. Boulineau, W. Porcher and B. Lestriez, *ACS Applied Materials and Interfaces*, 2019, **11**, 18331–18341.

10 I. A. Shkrob, J. A. Gilbert, P. J. Phillips, R. Klie, R. T. Haasch, J. Bareño and D. P. Abraham, *Journal of The Electrochemical Society*, 2017, **164**, A1489–A1498.

11 R. Jung, R. Morasch, P. Karayaylali, K. Phillips, F. Maglia, C. Stinner, Y. Shao-Horn and H. A. Gasteiger, *Journal of The Electrochemical Society*, 2018, **165**, A132.

12 Paulsen, *High nickel cathode material having low soluble base content*, 2012.

13 X. Zhang, W. J. Jiang, X. P. Zhu, A. Mauger, Qilu and C. M. Julien, *Journal of Power Sources*, 2011, **196**, 5102–5108.

14 D. Bresser, D. Buchholz, A. Moretti, A. Varzi and S. Passerini, *Energy and Environmental Science*, 2018, **11**, 3096–3127.

15 K. Sahni, M. Ashuri, Q. He, R. Sahore, I. D. Bloom, Y. Liu, J. A. Kaduk and L. L. Shaw, *Electrochimica Acta*, 2019, **301**, 8–22.

16 N. Loeffler, G. T. Kim, F. Mueller, T. Diemant, J. K. Kim, R. J. Behm and S. Passerini, *ChemSusChem*, 2016, **9**, 1112–1117.

17 W. Bauer, F. A. Çetinel, M. Müller and U. Kaufmann, *Electrochimica Acta*, 2019, **317**, 112–119.

18 M. Memm, A. Hoffmann and M. Wohlfahrt-Mehrens, *Electrochimica Acta*, 2018, **260**, 664–673.

19 C. H. Jo, D. H. Cho, H. J. Noh, H. Yashiro, Y. K. Sun and S. T. Myung, *Nano Research*, 2015, **8**, 1464–1479.

20 F. Lin, I. M. Markus, D. Nordlund, T.-C. Weng, M. D. Asta, H. L. Xin and M. M. Doeff, *Nature Communications 2014 5:1*, 2014, **5**, 1–9.

21 N. Loeffler, J. Von Zamory, N. Laszczynski, I. Doberdo, G. T. Kim and S. Passerini, *Journal of Power Sources*, 2014, **248**, 915–922.

22 E. Billy, M. Joulié, R. Laucournet, A. Boulineau, E. De Vito and D. Meyer, *ACS Applied Materials and Interfaces*, 2018, **10**, 16424–16435.

23 M. Jo, S. H. Park and H. Lee, *Materials (Basel, Switzerland)*, 2021, **14**, 4670.

24 C. Busà, M. Belekoukia and M. J. Loveridge, *Electrochimica Acta*, 2021, **366**, 137358.